

**NANO EXPRESS**

**Open Access**

# Shape-anisotropic enhanced damping in CoZr periodic arrays of nanohill structure

Fenglong Wang, Gaoxue Wang, Changjun Jiang\* and Desheng Xue

## Abstract

The preparation of CoZr nanostructure films to replicate the order of anodized aluminum oxide template with barrier layer was described. Coercivity and in-plane magnetic anisotropy were increased with the increase of oblique sputtering angle. Resonance frequency and damping factor had the same tendency also. Note that larger damping factor in nanostructure films was observed compared with that of continuous films in Si substrate, which was induced by magnetic anisotropy distribution particularly with a significant out-of-plane contribution due to the competition of shape anisotropy.

**Keywords:** Anodized aluminum oxide; Thin films; Nanohill structure

**PACS:** 75.75.-c, 75.70.-i, 07.57.Pt

## Background

It was known that working frequency is moving to the gigahertz band region for applications such as magnetic recording heads, wireless inductor cores, and microwave noise filters [1]. It requires the development of a soft magnetic film with high resonance frequency and high permeability [2,3]. In order to solve the expanded electromagnetic interference problems, many researchers begin to focus on the enhancement of microwave absorption [4]. Magnetic thin film application is based on the analysis of the dynamic magnetic or magnetization process, which is subjected to an effective magnetic anisotropy field  $H_{\text{eff}}$  as given by the Landau-Lifshitz-Gilbert (LLG) equation [5] and resonance frequency  $f_r$  [6]

$$\frac{dM}{dt} = -\gamma(M \times H_{\text{eff}}) + \frac{\alpha}{M_s} M \times \frac{dM}{dt} \quad (1)$$

$$f_r = \frac{\gamma}{2\pi} \sqrt{M_s H_{\text{eff}}} \quad (2)$$

where  $M_s$  represents saturation magnetization,  $H_{\text{eff}}$  is the anisotropy effective field,  $\gamma$  is the gyromagnetic factor, and  $\alpha$  is the damping constant. From Equations 1 and 2, it can be seen that magnetic anisotropy and

saturation magnetization are the two key material parameters which determine the magnetic properties of the magnetic film. The resonance frequency can be regulated through magnetic anisotropy. Generally, magnetic anisotropy is affected by many factors, such as demagnetization energy from the sample's shape or microstructure [7], magneto-crystalline energy from the material's crystal symmetry [8], magneto-elastic interactions from the stress state of the sample [9], single-ion anisotropy or pair order from chemical short-range order effect [10], exchange anisotropy from the ferromagnetic-antiferromagnetic coupling [11], etc. For thin films, in-plane uniaxial anisotropy determines microwave magnetic properties. Usually, uniaxial magnetic anisotropy is induced by many methods, for example, controlling the sputtering angle [12,13], changing the target-substrate distance [14], controlling the stress [9,15], using nanowire arrays [16], etc.

Ordered magnetic nanostructures, composed of arrays of different kinds of magnetic elements arranged in a periodic fashion, have attracted increasing attention in recent years [17,18]. Shape anisotropy was introduced with spatial dependence on a very small length scale when a periodic nanostructure is defined in a continuous magnetic thin film. The rapid advance in the fabrication of nanostructures, with controlled submicron size and shape offered by modern lithography techniques like ion or electron beam lithography, has triggered

\* Correspondence: jiangchj@lzu.edu.cn  
Key Lab for Magnetism and Magnetic Materials of the Ministry of Education, Lanzhou University, Lanzhou 730000, People's Republic of China

increased research on magnetic nanostructures (dots, stripe, or antidots) with a variety of shapes [19–21]. Anodized aluminum oxide (AAO) template with a high areal density [22,23] (up to 1,011 pores/cm<sup>2</sup>) and narrow size distribution over a large area has received much attention because of its simple and inexpensive control of structural parameters and excellent thermal and mechanical stability.

Various routes have been proposed to replicate the ordering of AAO where the final replicated nanostructures consist of highly ordered glassy antidots, nanowire, etc. In these nanostructured materials, large coercivity is induced due to strong shape anisotropy, which have attracted a great deal of interest owing to their potential applications as optoelectronics, data storage materials, surface modifiers with specific wetting behavior, etc. [24]. However, in order to apply magneto-electronic devices in the gigahertz region, a soft magnetic film with low coercivity and in-plane uniaxial anisotropy is developed. Therefore, in the present work, we use an AAO nanostructure with barrier layer as a substrate. CoZr

nanohill structured magnetic film (approximately 25 nm) has been sputtered onto a barrier layer of AAO by oblique sputtering. Oblique sputtering would induce in-plane uniaxial anisotropy [25] and increase shape anisotropy. We investigated static and dynamic magnetic properties of CoZr nanostructured films with various oblique sputtering angles and obtained adjustable resonance frequency and linewidth.

## Methods

The annealed aluminum foil (99.95%) was used to prepare the single anodic alumina template (AAO). Two-step oxidation was used to obtain the anodic alumina template. At the first step, Al was anodized in 0.3 M oxalic acid at 40 V for 1 h. Then the alumina from the first step was etched away by an alumina etchant (chromic acid and phosphoric acid) at 60°C for 30 min. At the second step, the oxidation was similar to the first step, but the oxidation time was 8 h.

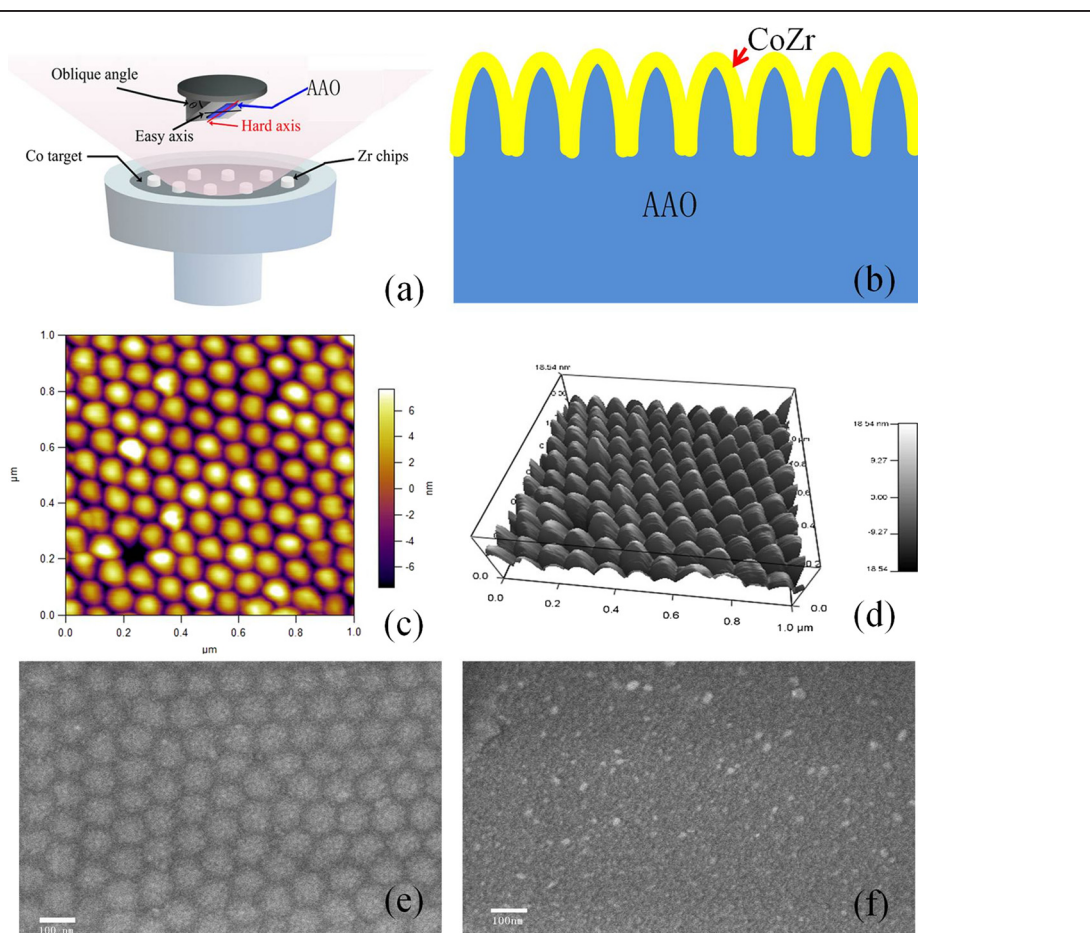


**Figure 1** The nanostructured thin film. (a) Schematic illustration of the sputtering arrangement. (b) Schematic of the layer structure. (c and d) AFM image of the barrier layer surface of the AAO template. SEM images of the (e) 0° and (f) 60° samples.

CoZr soft magnetic thin film was prepared by radio frequency sputtering onto the single anodic alumina template with a background pressure lower than  $6.0 \times 10^{-5}$  Pa, and a 0.2-MPa pressure of argon was used in the sputtering. A Co target, 70 mm in diameter and 3 mm in thickness, on which eight Zr chips were placed in a regular manner, was used as Figure 1a shows. The sputtering angle of the film was from 0° to 60°, every 20°. Growth rate at different oblique angles was different; we kept all samples 50-nm thick with adjusting of the sputtering time. Figure 1b shows the schematic of the layered structure. The surface morphology of the arrays was investigated with an atomic force microscope (AFM; MFP-3D(TM), Asylum Research, Goleta, CA, USA) and scanning electron microscope (SEM; Hitachi S-4800, Tokyo, Japan). The static magnetic properties of the samples were measured using a vibrating sample magnetometer (VSM). Out-plane ferromagnetic resonance (FMR) measurements were performed with a JEOL JES-FA 300 spectrometer (JEOL, Tokyo, Japan; X-band at 8.969 GHz). The microwave permeability measure-

ments of the films were performed using a vector network analyzer (PNA E8363B) with a microstrip method.

## Results and discussion

Figure 1c,d shows the AFM surface morphology of the barrier layer in the anodic alumina oxide template. From the figure, the barrier layer surface presented smooth mountains with heights of around 10 nm. In the template production process, the process parameters of template projection were oxidation voltage and electrolyte concentration. With the increase of oxidation voltage, the diameter of the projection increases; when electrolyte concentration increases, the current density increases, and there is increase in the diameter of the projection. The reason for the projections formed could be explained by the electric field under the support of the template oxidation process dissolution model [26]. The charge was the most concentrated at the bottom of the holes, and dissolution rate was the fastest. Figure 1e,f shows the SEM micrographs of the 0° and 60° samples. As shown from the figure, the sample of the oblique 0° kept the nanohill

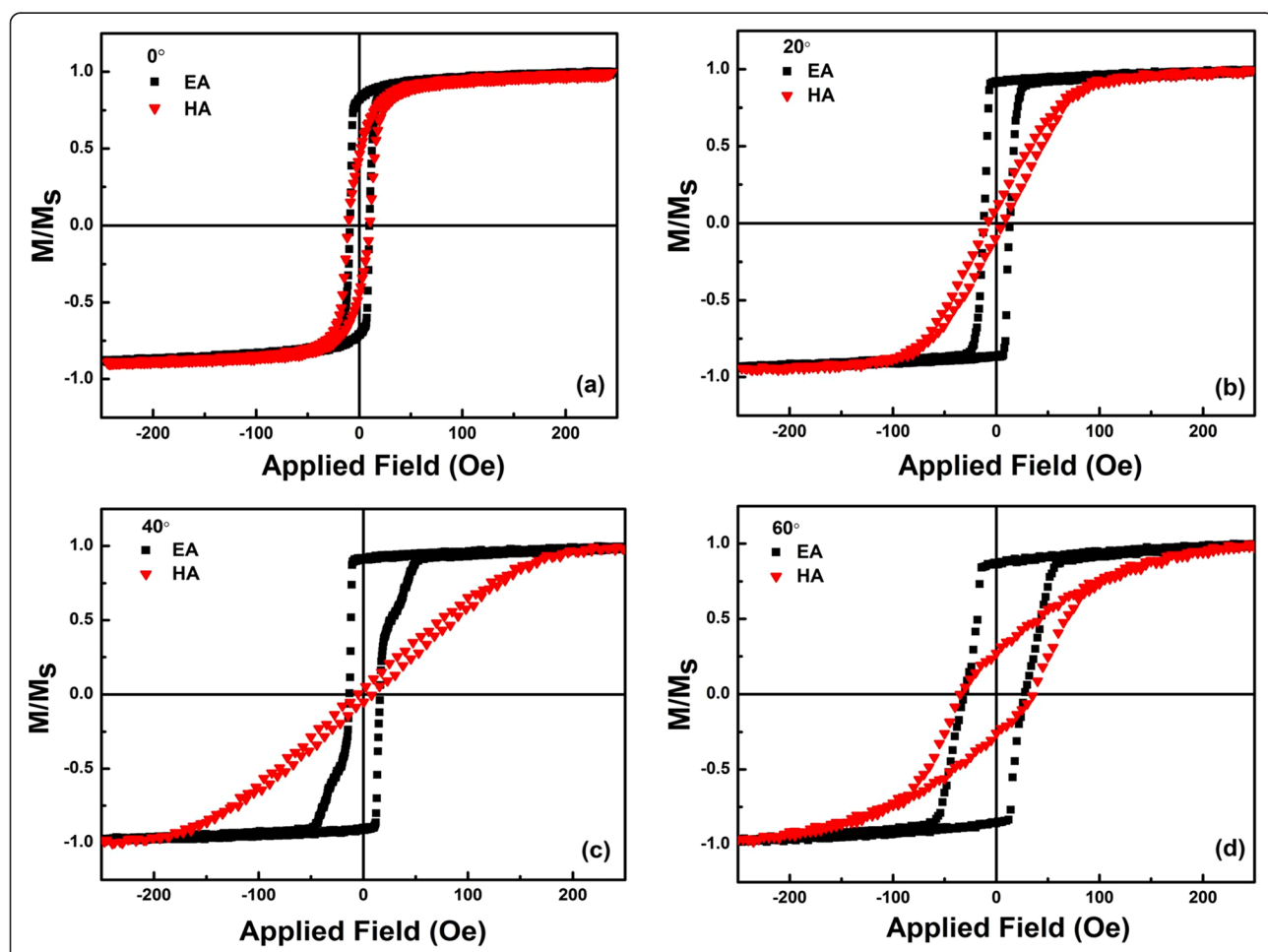


Figure 2  $M/M_s$  loops along both easy axes and hard axes. (a) 0°, (b) 20°, (c) 40°, and (d) 60° samples.

shape from replicating the order of an anodized aluminum oxide template with barrier layer; however, this nanostructure disappeared with oblique sputtering, as shown Figure 1f.

Figure 2 shows the magnetic hysteresis loops of the as-deposited CoZr thin films with oblique sputtering angle from 0° to 60° measured at room temperature, where the magnetic field was applied on the film plane. Note that for the sample with oblique sputtering angle of 0°, the results of the static magnetic measurements revealed that the as-deposited CoZr structured film possesses in-plane uniaxial anisotropy weakly. This was induced by uniaxial stress induced due to gradient sputtering [27]. Hysteresis loops of the easy magnetization direction were substantially a rectangle, while remanence ratio ( $M_r/M_s$ ) was close to 1. Moreover, the difference between easy and hard axis loops increased with the increase of oblique sputtering angle, which indicated change of magnetic anisotropy.

The overall dependences of anisotropy field  $H_k$  and coercivity of easy axis direction with various oblique sputtering angles were summarized in Figure 3. Here,  $H_k$  could be estimated by checking the cross point of the central line of the hard axis loop with the counter extension of the magnetization saturation line [28]. With increasing oblique sputtering angle, the coercivity in the easy axis ( $H_{ce}$ ) increased slightly from 10 to 27 Oe. In addition, the coercivity of nanostructure films was larger than that of continuous films [18,29], which was attributed to the change in the interaction of shape anisotropy and inhomogeneous magnetization rotation caused by the nanohill pattern of the magnetic films. As the angle increased,  $H_k$  increased monotonically, which was attributed to anisotropy induced by gradient sputtering and oblique sputtering. With increasing oblique sputtering angle, anisotropy

induced by oblique sputtering was increased and played a dominant role gradually. Therefore,  $H_k$  increased with increasing oblique sputtering angle.

Figure 4 shows the dependence of complex permeability  $\mu = \mu' - j\mu''$  on frequency for the films with different oblique sputtering angles measured by microstrip method using a vector network analyzer (PNA E8363B). The  $\mu'$  and  $\mu''$  represent the real and imaginary part of complex permeability. Due to weak magnetic anisotropy in the sample with an oblique sputtering angle of 0°, the curve of complex permeability depending on frequency was almost unchanged. Hence, the data was not included here. From Figure 4b, the peak of the imaginary complex permeability shifted to high frequency with increasing oblique sputtering angle. Furthermore, the linewidth of all samples was above 1 GHz, which was larger compared with that of continuous films at around 0.5 GHz [30]. Generally, the permeability spectra could be analyzed based on the LLG equation [5]; based on Equation 1, the permeability spectrum of magnetic thin film with in-plane uniaxial anisotropy can be expressed as [31]

$$\mu = 1 + \frac{\omega_m(\omega_0 + \omega_m + i\alpha\omega)}{\omega_r^2 - \omega^2 + i\alpha\Delta\omega_r} \quad (3)$$

with  $\omega_m = \gamma 4\pi M_s$ ,  $\omega_0 = \gamma H_k$ ,  $\omega_r^2 = \omega_0^2 + \omega_0\omega_{nr}$ ,  $\Delta\omega_r = \alpha(2\omega_0 + \omega_m)$ , where  $4\pi M_s$  is the saturation magnetization and takes the measurement value.

The permeability spectrum can be fitted with Equation 3, as shown by the solid lines in Figure 4b. The fitting parameters are plotted in Figure 4c. The resonance frequency ( $f_r$ ) increased from 2.9 to 4.2 GHz with the increase of oblique sputtering angle, which had the same tendency with that of  $H_k$ . The damping factor also increased from 0.015 to 0.165, which was larger than that of continuous films at around 0.01 [30]. Intrinsic damping and extrinsic sample inhomogeneities were two dominant contributions to the linewidth. The intrinsic LLG damping was generally a confluent process such as magnon-electron scattering. There was also extrinsic damping via two-magnon processes, such as the result of scattering from grain and grain boundaries, etc. Both the intrinsic and extrinsic processes lead to loss in the system. Besides the above two factors, an additional source of the linewidth was the sample inhomogeneities (not a real loss) which typically resulted in the distribution of material properties, such as the anisotropy, that would increase the linewidth. In order to understand the origin of the enhancement of the linewidth and/or damping factor, FMR was measured as a function of the angle between external magnetic field and in-plane easy axis.

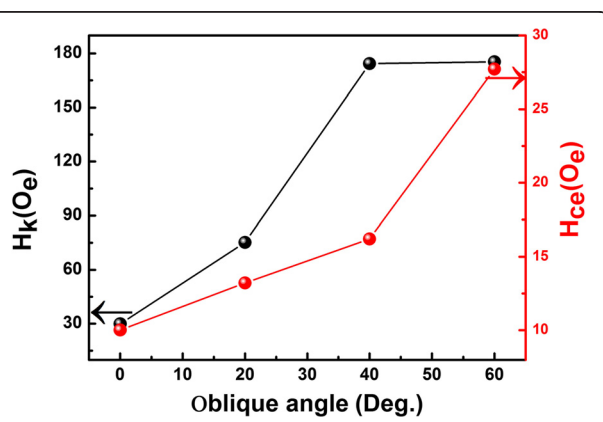
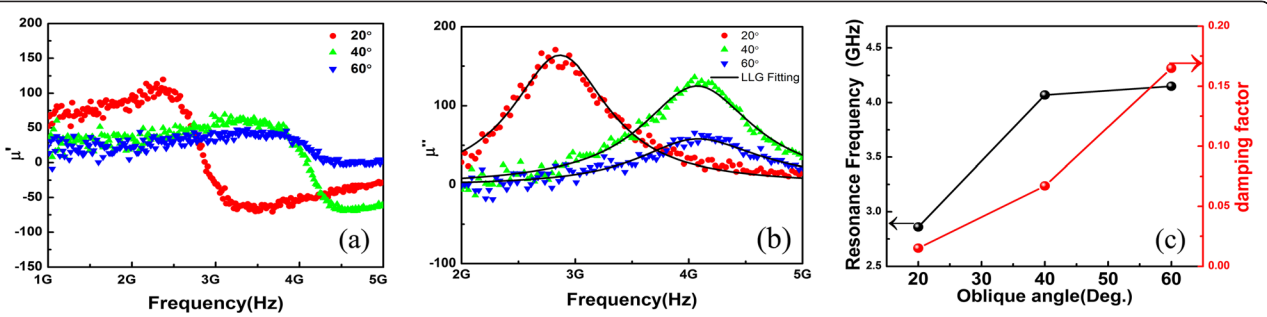


Figure 3 The static anisotropy effective field and the coercivity versus the oblique sputtering angle.



**Figure 4** Dependence of complex permeability  $\mu = \mu' - j\mu''$  on frequency for the films with different oblique sputtering angles.

Permeability spectra: the experimental results (symbols) and the fitting results by LLG equation (solid lines). (a)  $\mu'$ ; (b)  $\mu''$ . (c) Resonance frequency and damping factor versus oblique sputtering angle.

The ferromagnetic resonance equation for out-of-plane measurement configuration [32] is given as follows:

$$\left(\frac{\omega}{\gamma}\right)^2 = \left\{ H \cos(\theta_M - \theta_H) - \left(4\pi M_s - \frac{2K_\perp}{M_s}\right) \cos 2\theta_M \right\} \\ \times \left\{ H \cos(\theta_M - \theta_H) - \left(4\pi M_s - \frac{2K_\perp}{M_s}\right) \cos^2 \theta_M - \frac{2K_u}{M_s} \right\} \quad (4)$$

where  $\gamma$  is the gyromagnetic ratio,  $4\pi M_s$  is the saturation magnetization of the film,  $K_\perp$  is the perpendicular magnetic anisotropy constant,  $\theta_H$  is the angle between the

external field and film normal, and  $\theta_M$  is the angle between magnetization vector and film normal.

The measurement configuration was shown in the inset of Figure 5. The out-of-plane resonance field versus field orientation  $\theta_H$  for films deposited at an oblique sputtering angle of  $0^\circ$  and  $60^\circ$  is shown in Figure 5. The resonance fields decreased monotonically for each film with increasing angle between the external field  $H$  and the film normal, which was caused by the demagnetization energy when the external field  $H$  was parallel to film normal. Moreover, the magnitude of resonance field decreased with increasing oblique sputtering angle, which was closely related to the perpendicular anisotropy field  $2K_\perp/M_s$  in the first term on the right side

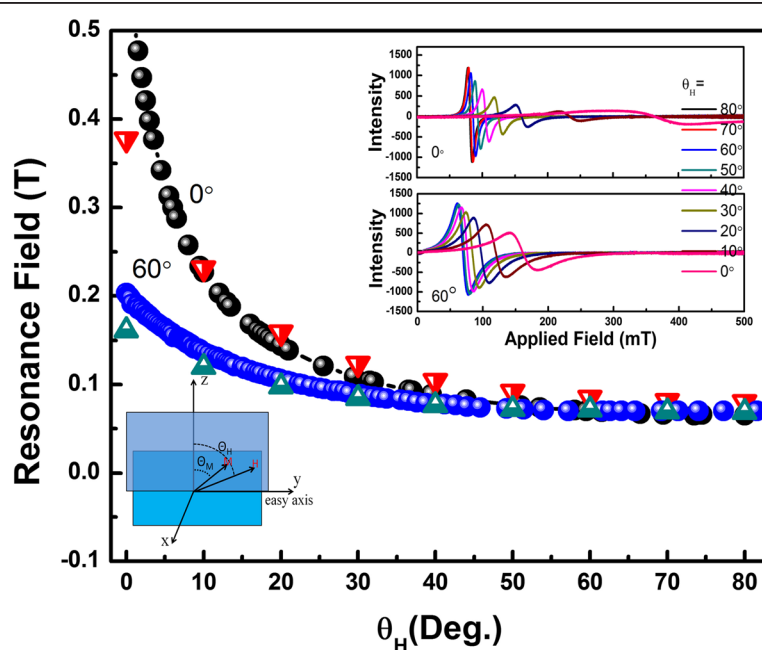


**Figure 5** Resonance field versus the angle between the external field and the easy axis. The circles represent the resonance fields for CoZr films deposited at a tilted substrate angle of  $0^\circ$  and  $60^\circ$ , respectively. The triangles are theoretical lines obtained by Equation 5. The insets are ESR of the samples with oblique sputtering angle of  $0^\circ$  and  $60^\circ$ .

of Equation 4. Taking into account the equilibrium equation of magnetization

$$H \sin(\theta M_0 - \theta H) - (4\pi M_s - 2K_\perp/M_s) \sin\theta M_0 \cos\theta M_0 = 0 \quad (5)$$

Here the saturation magnetization  $4\pi M_s$  was obtained by static VSM measurement; the perpendicular magnetic anisotropy constant could be acquired by fitting the experimental data with Equation 5. The fitted result showed that  $K_\perp$  of  $60^\circ$  was  $16.3 \times 10^3$  erg/cm $^3$  larger than the  $12.9 \times 10^3$  erg/cm $^3$  of  $0^\circ$ , which indicated increase with increasing oblique sputtering angle. Generally, the  $K_\perp$  of continuous film was almost zero due to strong demagnetization energy. In our case, the decrease of demagnetization energy was caused by shape anisotropy of nanostructure films, which induced the increase of  $K_\perp$ . Therefore, the increase of  $K_\perp$  induced inhomogeneities of magnetic anisotropy, which resulted in the increase of linewidth and/or damping factor.

## Conclusions

The static and dynamic magnetic properties of CoZr/AAO films with different oblique sputtering angles have been investigated. All the properties and parameters were found to be dependent on magnetic anisotropy field which was induced by the shape of the AAO template and oblique sputtering. The competition between the two factors resulted in the trend of dependence on anisotropy field  $H_k$  and remanence ratio  $M_r/M_s$ , with various oblique sputtering angles. The resonance frequency change of CoZr/AAO films was also attributed to the effect of properties and oblique sputtering. Enhanced microwave absorption was confirmed by complex permeability measurement comparing with continuous film on a Si substrate.

## Abbreviations

AAO: Anodized aluminum oxide; AFM: Atomic force microscope; SEM: Scanning electron microscope; VSM: Vibrating sample magnetometer; FMR: Ferromagnetic resonance.

## Competing interests

The authors declare that they have no competing interests.

## Authors' contributions

FW fabricated the CoZr films, performed the measurements, and wrote the manuscript. CJ analyzed the results and wrote the manuscript. GW helped to grow and measure the films. DX supervised the overall study. All authors read and approved the final manuscript.

## Acknowledgments

This work is supported by the National Basic Research Program of China (grant no. 2012CB933101), the National Science Fund for Distinguished Young Scholars (grant no. 50925103), and the National Natural Science Foundation of China (grant no. 11034004 and 50902064).

Received: 3 April 2013 Accepted: 7 June 2013

Published: 12 June 2013

## References

1. Encinas-Oropesa A, Demand M, Piraux L, Ebels U, Huynen I: Effect of dipolar interactions on the ferromagnetic resonance properties in arrays of magnetic nanowires. *J Appl Phys* 2001, **89**:6704.
2. Fish GE: Soft magnetic materials. *Proc IEEE* 1990, **78**:947–972.
3. Yamaguchi M, Suezawa K, Arai KI, Takahashi Y, Kikuchi S, Shimada Y, Li WD, Tanabe S, Ito K: Microfabrication and characteristics of magnetic thin-film inductors in the ultrahigh frequency region. *J Appl Phys* 1999, **85**:7919.
4. Che RC, Peng LM, Duan XF, Chen Q, Liang XL: Microwave absorption enhancement and complex permittivity and permeability of Fe encapsulated within carbon nanotubes. *Adv Mater* 2004, **16**:401–405.
5. Gilbert TL: Classics in magnetics a phenomenological theory of damping in ferromagnetic materials. *IEEE Trans Magn* 2004, **40**:3443–3449.
6. Kittel C: On the gyromagnetic ratio and spectroscopic splitting factor of ferromagnetic substances. *Phys Rev* 1949, **76**:743–748.
7. Kaczer J, Murtinová L: On the demagnetizing energy of periodic magnetic distributions. *Phys Status Solidi A* 1974, **23**:79–86.
8. Asdente M, Delitala M: Magnetocrystalline energy, electronic charge distribution, and fermi surface of iron from a tight-binding calculation. *Phys Rev* 1967, **163**:497–503.
9. Naik R, Poli A, McKague D, Lukaszew A, Wenger L: Strain-induced perpendicular magnetic anisotropy of <100>-oriented Ni-Cu superlattices. *Phys Rev B* 1995, **51**:3549–3553.
10. Jaswal S: Comment on "Generic source of perpendicular anisotropy in amorphous rare-earth-transition-metal films". *Phys Rev Lett* 1992, **68**:1440–1440.
11. Malozemoff AP: Random-field model of exchange anisotropy at rough ferromagnetic-antiferromagnetic interfaces. *Phys Rev B* 1987, **35**:3679–3682.
12. Wehner G: Influence of the angle of incidence on sputtering yields. *J Appl Phys* 1959, **30**:1762.
13. Sugai I, Oyaizu M, Takeda Y, Kawakami H, Hattori H, Kawasaki K: Influence of carbon material and sputtering angle on stripper foil lifetime. *Nucl Instrum Methods Phys* 2010, **613**:448–452.
14. Fu Y, Yang Z, Miyao T, Matsumoto M, Liu XX, Morisako A: Induced anisotropy in soft magnetic Fe<sub>65</sub>Co<sub>35</sub>/Co thin films. *Mater Sci Eng: B* 2006, **133**:61–65.
15. Fan Y, Zhao HB, Lüpke G, Hanbicki AT, Li CH, Jonker BT: Anisotropic exchange coupling and stress-induced uniaxial magnetic anisotropy in Fe/GaAs(001). *Phys Rev B* 2012, **85**:165311.
16. Vivas L, Vazquez M, Escrig J, Allende S, Altbir D, Leitao D, Araujo J: Magnetic anisotropy in CoNi nanowire arrays: analytical calculations and experiments. *Phys Rev B* 2012, **85**:035439.
17. Rahman MT, Shams NN, Lai CH, Fidler J, Suess D: Co/Pt perpendicular antidot arrays with engineered feature size and magnetic properties fabricated on anodic aluminum oxide templates. *Phys Rev B* 2010, **81**:014418.
18. Jiang C, Wei W, Liu Q, Guo D, Xue D: Magnetic irreversibility of the Fe antidot arrays film by depositing on the porous alumina templates. *Appl Surf Sci* 2012, **258**:3723–3725.
19. Gago R, Vázquez L, Plantevin O, Sánchez-García JA, Varela M, Ballesteros MC, Albella JM, Metzger TH: Temperature influence on the production of nanodot patterns by ion beam sputtering of Si(001). *Phys Rev B* 2006, **73**:155414.
20. Maruyama R, Yamazaki D, Ebisawa T, Soyama K: Development of high-reflectivity neutron supermirrors using an ion beam sputtering technique. *Nucl Instrum Methods Phys* 2009, **600**:68–70.
21. Völner J, Ziberi B, Frost F, Rauschenbach B: Topography evolution mechanism on fused silica during low-energy ion beam sputtering. *J Appl Phys* 2011, **109**:043501.
22. Sung K, Jae L, Young C, Sung H, Kyung Y: Reversible resistive switching behaviors in NiO nanowires. *Appl Phys Lett* 2008, **93**:033503.
23. Fathi R, Sanjabi S, Bayat N: Synthesis and characterization of NiMn alloy nanowires via electrodeposition in AAO template. *Mater Lett* 2012, **66**:346–348.
24. Byun J, Lee JI, Kwon S, Jeon G, Kim JK: Highly ordered nanoporous alumina on conducting substrates with adhesion enhanced by surface modification: universal templates for ultrahigh-density arrays of nanorods. *Adv Mater* 2010, **22**:2028–2032.
25. Wang G, Dong C, Wang W, Wang Z, Chai G, Jiang C, Xue D: Observation of rotatable stripe domain in permalloy films with oblique sputtering. *J Appl Phys* 2012, **112**:093907.

26. Ma Zhi W, Qin SX, Jian W, Chuan W, Xiang L: Deposition of diamond films on copper substrate. *Plasma Sci Technol* 2000, **2**:207–212.
27. Li S, Huang Z, Duh J-G, Yamaguchi M: Ultrahigh-frequency ferromagnetic properties of FeCoHf films deposited by gradient sputtering. *Appl Phys Lett* 2008, **92**:092501.
28. Xu F, Liao Z, Huang Q, Ong CK, Li S: Influence of interlayer thickness on high-frequency magnetic properties of FeCoSiN/AIO/FeCoSiN trilayers. *IEEE Trans Magn* 2011, **47**:3100–3103.
29. Chang HW, Wu MH, Hsieh CC, Chang WC, Xue DS: High magnetic anisotropy field in CoZr thin films. *IEEE Trans Magn* 2011, **47**:3924–3927.
30. Jiang C, Xue D, Guo D, Fan X: Adjustable resonance frequency and linewidth by Zr doping in Co thin films. *J Appl Phys* 2009, **106**:103910.
31. Ben Youssef J, Vukadinovic N, Billeter D, Labrunie M: Thickness-dependent magnetic excitations in permalloy films with nonuniform magnetization. *Phys Rev B* 2004, **69**:174402.
32. Diaz de Sihues M, Durante-Rincón CA, Fermin JR: A ferromagnetic resonance study of NiFe alloy thin films. *J Magn Magn Mater* 2007, **316**:462–465.

doi:10.1186/1556-276X-8-284

**Cite this article as:** Wang et al.: Shape-anisotropic enhanced damping in CoZr periodic arrays of nanohill structure. *Nanoscale Research Letters* 2013 **8**:284.

Submit your manuscript to a SpringerOpen® journal and benefit from:

- Convenient online submission
- Rigorous peer review
- Immediate publication on acceptance
- Open access: articles freely available online
- High visibility within the field
- Retaining the copyright to your article

Submit your next manuscript at ► [springeropen.com](http://springeropen.com)